

# Effect of Surface Charge of Immortalized Mouse Cerebral Endothelial Cell Monolayer on Transport of Charged Solutes

WEI YUAN, GUANGLEI LI, and BINGMEI M. FU

Department of Biomedical Engineering, The City College of the City University of New York, 138th Street at Convent Avenue, New York, NY 10031, USA

(Received 6 September 2009; accepted 7 January 2010; published online 20 January 2010)

Associate Editor Julia E. Babensee oversaw the review of this article.

**Abstract**—Charge carried by the surface glycocalyx layer (SGL) of the cerebral endothelium has been shown to significantly modulate the permeability of the blood–brain barrier (BBB) to charged solutes *in vivo*. The cultured monolayer of bEnd3, an immortalized mouse cerebral endothelial cell line, is becoming a popular *in vitro* BBB model due to its easy growth and maintenance of many BBB characteristics over repeated passages. To test whether the SGL of bEnd3 monolayer carries similar charge as that in the intact BBB and quantify this charge, which can be characterized by the SGL thickness ( $L_f$ ) and charge density ( $C_{mf}$ ), we measured the solute permeability of bEnd3 monolayer to neutral solutes and to solutes with similar size but opposite charges: negatively charged  $\alpha$ -lactalbumin (−11) and positively charged ribonuclease (+3). Combining the measured permeability data with a transport model across the cell monolayer, we predicted the  $L_f$  and the  $C_{mf}$  of bEnd3 monolayer, which is ~160 nm and ~25 mEq/L, respectively. We also investigated whether orosomucoid, a plasma glycoprotein modulating the charge of the intact BBB, alters the charge of bEnd3 monolayer. We found that 1 mg/mL orosomucoid would increase SGL charge density of bEnd3 monolayer to ~2-fold of its control value.

**Keywords**—Blood–brain barrier, bEnd3, Surface glycocalyx layer, Monolayer permeability, Nanoparticles.

## INTRODUCTION

To protect brain from blood-borne neural toxins, the blood–brain barrier (BBB) between the central nervous system and the cerebral circulation maintains very low permeability due to its unique structure. In addition to endothelial cells with tight junctions, the BBB has complete wrapping of a very thin basement

membrane and astrocytic end-feet.<sup>15,24</sup> Various *in vivo* and *in vitro* models have been used for the study of the solute transport across the BBB. Except their comparatively high permeability and the loss of some expression of BBB efflux protein systems,<sup>32</sup> *in vitro* models have several advantages over *in vivo* models, including low cost, high-throughput screening, and easiness to assess compounds and to investigate the transport mechanism at molecular levels. Over decades, many *in vitro* models have been derived from primary brain capillary endothelial cell cultures, which have the closest resemblance to BBB phenotype *in vivo*,<sup>32</sup> and exhibit excellent characteristics of the BBB at early passages. However, primary cell cultures have their inherent disadvantages. For instance, they are usually extremely time consuming and require high skilled researchers. In addition, primary cell cultures lose their differential phenotype over repeated passages.<sup>32,33</sup> Moreover, primary cell cultures have potential contaminations from other types of brain cells such as pericytes and astrocytes, which induce leaky barriers in the *in vitro* monolayer models.<sup>8</sup> Recently, the *in vitro* monolayer deriving from immortalized mouse brain endothelial cell line, bEnd3, becomes popular because of its advantages over primary cell culture, including the ability to maintain BBB characteristics over many passages, as well as easy growth and low cost. Previous studies have evaluated bEnd3 cells as an *in vitro* BBB model in terms of expression of tight junction proteins, the permeability to sucrose, the trans-endothelial electrical resistance (TEER) as well as transporter of glucose.<sup>8,33</sup> These studies concluded that bEnd3 monolayer is an attractive *in vitro* BBB model, which can express mRNA for a number of important tight junction proteins, ZO-1, ZO-2, claudin-1, and claudin-3 and exhibit similar barrier functions as primary culture cells. In the

Address correspondence to Bingmei M. Fu, Department of Biomedical Engineering, The City College of the City University of New York, 138th Street at Convent Avenue, New York, NY 10031, USA. Electronic mail: fu@ccny.cuny.edu

present study, we investigated whether or not the bEnd3 monolayer is a good *in vitro* model for studying solute and nanoparticle transport across the BBB, especially the transport of charged molecules.

The surface glycocalyx layer (SGL) of the BBB is located on the luminal surface of the endothelium<sup>43</sup> and contains a great number of solid-bound fixed negative charge.<sup>39,41,45</sup> In addition to the tight junctions in between endothelial cells, the SGL plays an important role in maintaining the barrier function of endothelium due to its matrix-like structure as well as the charge.<sup>1,9,11,18,39,44</sup> Yuan *et al.*<sup>46</sup> found that the permeability of intact rat pial microvessels to positively charged ribonuclease was four times as large as that to negatively charged  $\alpha$ -lactalbumin, though they have almost the same size. Combining these measured permeability data with a mathematical model, they predicted that the charge density is  $\sim 30$  mEq/L in the structural components of the BBB, i.e., the SGL and the basement membrane. Therefore, the first objective of the present study is to test whether bEnd3 monolayer expresses the functional SGL as in the intact BBB by quantifying the thickness ( $L_f$ ) and charge density ( $C_{mf}$ ) of the cultured bEnd3 monolayer (Fig. 1). To do this, we measured the solute permeability of bEnd3 monolayer to fluorescently-labeled neutral solutes (sodium fluorescein and various sized dextrans) and charged solutes ( $\alpha$ -lactalbumin and ribonuclease). By utilizing a transport model across the bEnd3 monolayer with the measured permeability data, we can predict  $L_f$  and  $C_{mf}$  of the SGL at the bEnd3 monolayer.

Orosomucoid, a plasma glycoprotein, which is synthesized in the liver and may be also secreted by endothelial cells,<sup>38</sup> increases several folds during infection or trauma.<sup>29,35</sup> Orosomucoid is also bound to

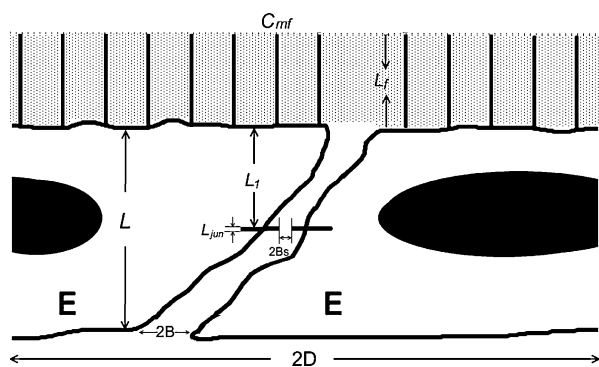


**FIGURE 1.** The schematic diagram of bEnd3 monolayer. There is a cleft (width  $2B$ ) with a tight junction (opening width  $2B_s$  and thickness  $L_{jun}$ ) in between two adjacent endothelial cells (Es). The thickness of the endothelial cell is  $L$  and the distance between the luminal side of the endothelial cell and the tight junction is  $L_1$ . At the luminal side of the endothelium, there is a surface glycocalyx layer with a thickness  $L_f$  and a charge density  $C_{mf}$ .

the surface of cultured bovine pulmonary microvascular endothelial cells.<sup>36</sup> It has been found that orosomucoid modulates the transport of charged solutes across the wall of peripheral and cerebral microvessels *in vivo* by decreasing the transport of negatively charged molecules but increasing that of positively charged ones,<sup>13,23,46</sup> suggesting that orosomucoid plays an essential role in maintaining the permeability property of endothelium by adding negative charge to the SGL.<sup>13,23,38</sup> The second objective of the present study is thus to investigate whether orosomucoid modulates the bEnd3 monolayer permeability in a similar way as it does for the intact endothelium of the BBB.

The third objective is to test whether or not bEnd3 cell monolayer is a good *in vitro* model for studying the transport of nanoparticle drug carriers across the BBB. In the past decade, the charge-loaded polymeric nanoparticles have attracted increasing interests as the carriers for therapeutic agents across the BBB due to their prolonged bioavailability, high loading efficiency, and tunable surface chemistry.<sup>31</sup> Gil *et al.*<sup>20</sup> developed novel quaternary ammonium  $\beta$ -cyclodextrin (QA $\beta$ CD) nanoparticles as drug delivery carriers across the BBB. The QA $\beta$ CD nanoparticles exhibit cationic property, which has been considered as an effective approach to enhance the transport across the BBB.<sup>26</sup> The hydrodynamic radii of QA $\beta$ CD nanoparticles are from 65 to 88 nm in pH 7.4 and 37 °C,<sup>20</sup> which are significantly larger than the size of paracellular pathways of the BBB. Surprisingly, Gil *et al.*<sup>20</sup> found that the permeability of the bovine brain microvessel endothelial cell (BBMEC) monolayer to QA $\beta$ CD nanoparticles was either comparable or even larger than that to neutral dextran-4k, whose molecular weight is similar to that of one basic unit of QA $\beta$ CD nanoparticles ( $\sim 5000$ ). One explanation was that when the large QA $\beta$ CD nanoparticle crosses the BBMEC monolayer, it degrades to its much smaller basic units. Another more likely explanation was that the transport of the nanoparticles is by transcytosis, a trans-cellular process, instead of through a paracellular pathway. To examine whether or not bEnd3 monolayer is able to mimic the transport of nanoparticles across the endothelium of the intact BBB, we measured the bEnd3 monolayer permeability to these QA $\beta$ CD nanoparticles, and compared with that of intact rat pial microvessels.

## MATERIALS AND METHODS

### Cell Culture

Immortalized mouse cerebral endothelial cells, bEnd3 cells (American Type Culture Collection,

Manassas, VA) were grown in DMEM with 4.5 g/L glucose, 10% FBS, 3.7 g/L sodium bicarbonate, and 4 mM glutamine. Cells were maintained in a humidified cell culture incubator at 37 °C and with 5% CO<sub>2</sub>/95% room air. Cells used in all experiments were in passage 28–35. Cells were seeded at a density of  $6.0 \times 10^4$  cells/cm<sup>2</sup> on Transwell permeable inserts (12 mm in diameter, 0.4 μm pores size; Corning Incorporated, Corning, NY). Inserts were incubated at 37 °C with 200 μL of 30 μg/mL fibronectin for 1 h before plating cells. The cells seeded onto Transwell insert reached confluence within approximately two days, shown in Fig. 2, in which the tight junction accessory proteins ZO-1 were stained with anti-ZO-1 antibody in green and the nuclei of endothelial cells were stained with propidium iodide in red. The permeability experiments were performed on the monolayer 4–5 days after cell seeding, allowing sufficient

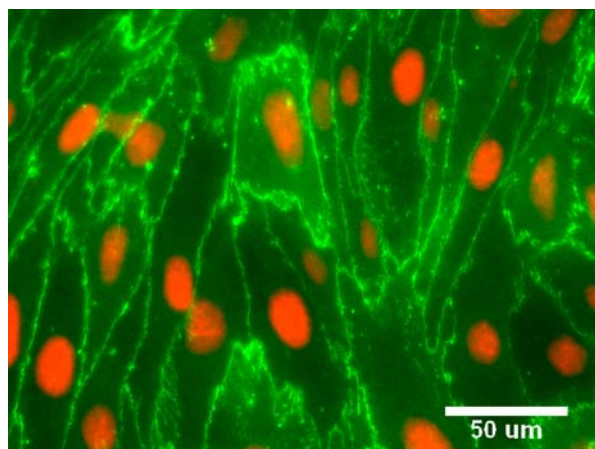


**FIGURE 2.** bEnd3 cells grown on a Transwell insert were observed using a fluorescence microscope, in which tight junction accessory proteins ZO-1, were stained with anti-ZO-1 antibodies in green and the nuclei of endothelial cells were stained with propidium iodide in red.

time for the cells to develop the junctions between cells.

#### *In Vitro Solute Permeability Measurement*

On the day of experiment, Transwell insert filter was washed with PBS, and then the media of the donor chamber was filled with 0.5 mL fluorescently-labeled test solutes in Ringer solution containing 10 mg/mL BSA while the acceptor chamber was filled with 1.5 mL Ringer solution containing 10 mg/mL BSA (Fig. 3). The samples of 50 μL were drawn every 10 min for 90 min from the acceptor chamber and were then replaced with the same amount of Ringer-BSA solution. The fluorescence tracer concentration in the samples was determined by Bio-Tek Synergy HT plate reader (Winooski, VT), and the excitation and emission wavelengths were set to 485 and 535 nm, respectively, for all fluorescence tracers in the present study. The solute permeability ( $P$ ) of the monolayer was calculated from the relationship,

$$P = \frac{\Delta C_A}{\Delta t} \times \frac{V_A}{C_D \times S}$$

where  $\Delta C_A/\Delta t$  is the increase in fluorescence concentration in the acceptor chamber during the time interval  $\Delta t$ ,  $C_D$  is fluorescence concentration in the donor chamber (assumed to be constant during the experiment),  $V_A$  is the volume of the acceptor chamber, and  $S$  is the surface area of the filter.

The measured solute permeability was made on the bEnd3 monolayer that was formed on Transwell insert with 0.4 μm pores. Transwell insert itself could also provide resistance on transport of solutes. Therefore, the total resistance of this *in vitro* model system comprises of two parts: the resistance from the monolayer and the resistance from the empty insert,

$$\frac{1}{P_t} = \frac{1}{P_c} + \frac{1}{P_i}$$

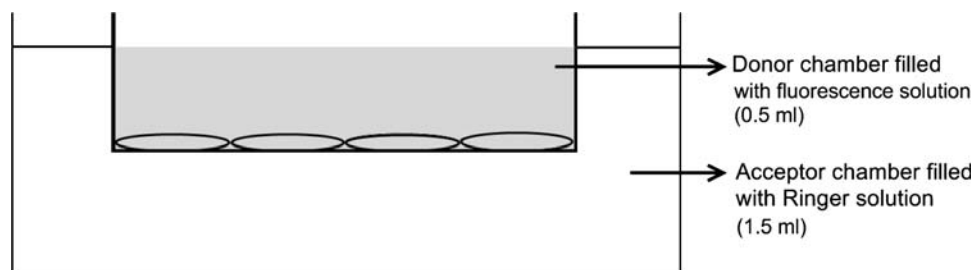


**FIGURE 3.** Transwell filter set-up for measuring bEnd3 monolayer permeability to solutes. The acceptor chamber was filled with 10 mg/mL BSA in Ringer solution, while the donor chamber was filled with the same solution added with fluorescently labeled solutes. The sample solution was extracted from the acceptor chamber every 10 min for fluorescence assessment and then was replaced with same amount of Ringer solution containing 10 mg/mL BSA.

Solving above equation, we have the permeability of the monolayer  $P_c$ ,

$$P_c = \frac{P_t}{1 - \frac{P_i}{P_t}}$$

Here  $P_t$  is the measured permeability of the total system and  $P_i$  is the permeability of the insert.

### *Solutions and Fluorescent Test Solute Preparation*

#### *Mammalian Ringer Solution*

Mammalian Ringer solution with 10 mg/mL bovine serum albumin (BSA, A4378, Sigma) was used during the permeability measurement. The solution composition was (in mM) NaCl 132, KCl 4.6, MgSO<sub>4</sub> 1.2, CaCl<sub>2</sub> 2.0, NaHCO<sub>3</sub> 5.0, glucose 5.5 and HEPES 20. All these chemicals were from Sigma. The pH was buffered to 7.4–7.45 by adjusting the ratio of HEPES acid to base. In addition, both the washout solution and the fluorescent dye solution contained bovine serum albumin (BSA, A4378, Sigma) at 10 mg/mL.<sup>19</sup> The solutions were made fresh on the day of use to avoid binding to the serum albumin.<sup>3,16</sup>

#### *Neutral Test Solutes: Sodium Fluorescein and FITC-Dextrans*

Sodium fluorescein (NaF; F6377, Sigma; mol. wt. 376, Stokes–Einstein radius ~0.45 nm) and all FITC-dextrans, FITC-dextran-4k (FD4, Sigma; mol. wt. 4000, Stokes radius ~1.4 nm), FITC-dextran-20k (FD20 s, Sigma; mol. wt. 20,000, Stokes radius ~2.4 nm), and FITC-dextran-70k (FD70 s, Sigma; mol. wt. 70,000, Stokes radius ~3.6 nm), were dissolved in Ringer solution containing 10 mg/mL BSA at the concentration of 10 μM.

#### *Charged Test Solutes: FITC-Labeled Ribonuclease and α-Lactalbumin*

Ribonuclease A (R5500, Sigma) and α-lactalbumin (L6010, Sigma) were labeled with FITC (F7250, Sigma, mol. wt. 389.4) as follows.<sup>2,16</sup> Protein (90 mg) was dissolved in 15 mL of borate buffer (0.05 M, pH approximately 9.3, 20 °C) containing 0.4 M NaCl. The solution was placed in 18-mm-diameter dialysis tubing (Spectrum Medical Industries, 3500 mol. wt. cutoff) and was then dialyzed for 12 h with constant stirring at 15 °C against 50 mL of the borate buffer containing FITC (0.5 mM). The labeled protein then was dialyzed against 2 L of glucose-free mammalian Ringer solution twice, each round for 12 h. The dialysis procedure was then performed twice with 2 L of normal Ringer solution until there was no free dye. The influence of the free dye on measured

permeability to a labeled protein was discussed by Fu *et al.*<sup>16</sup> The FITC-labeled α-lactalbumin and ribonuclease were stored frozen and used within 2 week of preparation. In addition, on the day of experiment, unlabeled 10 mg/mL BSA was added to aliquots of the labeled protein in the Ringer solution. The final FITC-α-lactalbumin and FITC-ribonuclease dye concentrations used in the experiment were 1 mg/mL in the Ringer-BSA solution. For this preparation, the fluorescence intensity of the free FITC dye was less than 1% of the solution, which was checked using the image system at the same instrument settings used in our *in vitro* experiments. All dye solutions described above were kept chilled until just before use and were discarded at the end of the day.

### *Analysis and Statistics*

All data were presented as means ± SE or otherwise specified. Data were analyzed for statistical significance using ANOVA. Significance was assumed for probability levels  $p < 5\%$ .

## **RESULTS AND DISCUSSION**

It has been demonstrated that bEnd3 monolayer is able to mimic permeability properties of primary culture models of early passages.<sup>8,33</sup> However, it was also suggested that the permeability of bEnd3 monolayer to sucrose increased significantly after passage 35, compared with that of prior passages. In the present study, we measured solute permeability of bEnd3 monolayer of the cells at passages from 28 to 35, 2–3 days after the formation of confluence. The extra time after confluence is crucial for the formation of the tight junctions between endothelial cells.<sup>8</sup>

#### *Solute Permeability of bEnd3 Monolayer to Neutral Solutes*

Table 1 summarized the measured permeability ( $P$ ) of the monolayer to sodium fluorescein and various sized neutral dextrans in Ringer-BSA solution. The solute permeability was also corrected by subtracting the resistance contributed by empty Transwell insert using the equation shown in the previous section. After correction, the permeability to sodium fluorescein ( $P^{\text{NaF}}$ ) was  $7.24 \pm 0.84 \times 10^{-6}$  cm/s, ranging from 5.40 to  $8.35 \times 10^{-6}$  cm/s, while  $P^{\text{Dex4k}}$  was  $2.91 \pm 0.43 \times 10^{-6}$  cm/s, ranging from 2.48 to  $4.01 \times 10^{-6}$  cm/s,  $P^{\text{Dex20k}}$  was  $0.80 \pm 0.16 \times 10^{-6}$  cm/s, ranging from 0.59 to  $1.04 \times 10^{-6}$  cm/s, and  $P^{\text{Dex70k}}$  was  $0.44 \pm 0.16 \times 10^{-6}$  cm/s, ranging from 0.26 to  $0.96 \times 10^{-6}$  cm/s.

**TABLE 1. Measured and corrected permeability ( $P$ ) of bEnd3 monolayer to neutral solutes.**

Solutes	MW	Stokes radius (nm)	$P$ ( $\times 10^{-6}$ cm/s), measured ( $\pm$ SE, $n = 6$ )	$P$ ( $\times 10^{-6}$ cm/s), corrected ( $\pm$ SE, $n = 6$ )
NaF	376	0.45	5.70 ( $\pm$ 0.66)	7.24 ( $\pm$ 0.84)
Dex4k	4000	1.4	2.38 ( $\pm$ 0.35)	2.91 ( $\pm$ 0.43)
Dex20k	20000	2.4	0.77 ( $\pm$ 0.15)	0.80 ( $\pm$ 0.16)
Dex70k	70000	3.6	0.42 ( $\pm$ 0.15)	0.44 ( $\pm$ 0.16)

**TABLE 2. Measured and corrected permeability ( $P$ ) of bEnd3 monolayer to charged solutes.**

Solutes	MW	Stokes radius (nm)	Solution in Transwell	$P$ ( $\times 10^{-6}$ cm/s), measured ( $\pm$ SE)	$P$ ( $\times 10^{-6}$ cm/s), corrected ( $\pm$ SE)
Ribonuclease	13,683	2.0	BSA	1.97 ( $\pm$ 0.56) $n = 6$	2.21 ( $\pm$ 0.63) $n = 6$
			Orosomuroid	3.24 ( $\pm$ 0.59) $n = 9$	3.95 ( $\pm$ 0.72) $n = 9$
$\alpha$ -Lactalbumin	14,176	2.01	BSA	1.03 ( $\pm$ 0.60) $n = 9$	1.09 ( $\pm$ 0.64) $n = 9$
			Orosomuroid	0.73 ( $\pm$ 0.26) $n = 9$	0.76 ( $\pm$ 0.27) $n = 9$

These values are comparable to those measured in previous studies of bEnd3 monolayer and other *in vitro* BBB models using primary cells for similar size solutes.<sup>7,8,21,33</sup>

#### Solute Permeability of bEnd3 Monolayer to Charged Solutes in the Presence and Absence of Orosomuroid

We measured permeability of bEnd3 monolayer to FITC-labeled  $\alpha$ -lactalbumin (MW 14,176; Stokes radius 2.01 nm; net charge  $-11$ ) and ribonuclease (MW 13,683; Stokes radius 2.0 nm; net charge  $+3$ ) in Ringer-BSA solution (control), and in that with additional 1 mg/mL orosomuroid (G3643,  $\alpha_1$ -acid glycoprotein, Sigma). Table 2 summarizes the measured and the corrected permeability to  $\alpha$ -lactalbumin and ribonuclease for both control and orosomuroid groups. After correction for the resistance from the Transwell insert, the permeability of the bEnd3 monolayer to ribonuclease in Ringer-BSA ( $P^{\text{ribonuclease, BSA}}$ ) was  $2.21 \pm 0.63 \times 10^{-6}$  cm/s, ranging from  $1.63$  to  $3.43 \times 10^{-6}$  cm/s, while the permeability to ribonuclease in the presence of orosomuroid ( $P^{\text{ribonuclease, ORO}}$ ) was  $3.95 \pm 0.72 \times 10^{-6}$  cm/s, ranging from  $2.48$  to  $4.91 \times 10^{-6}$  cm/s; Similarly,  $P^{\alpha\text{-lactalbumin, BSA}}$  was  $1.09 \pm 0.64 \times 10^{-6}$  cm/s, ranging from  $0.33$  to  $2.50 \times 10^{-6}$  cm/s, while  $P^{\alpha\text{-lactalbumin, ORO}}$  was  $0.76 \pm 0.27 \times 10^{-6}$  cm/s, ranging from  $0.42$  to  $1.14 \times 10^{-6}$  cm/s. Correspondingly, the ratio of permeability of the monolayer to positively charged ribonuclease to that to negatively charge  $\alpha$ -lactalbumin was 2.03 in the absence of orosomuroid, while this ratio increased to 5.20 in the presence of orosomuroid.

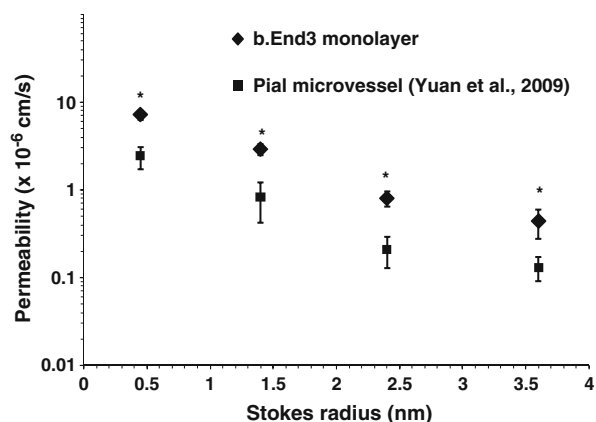


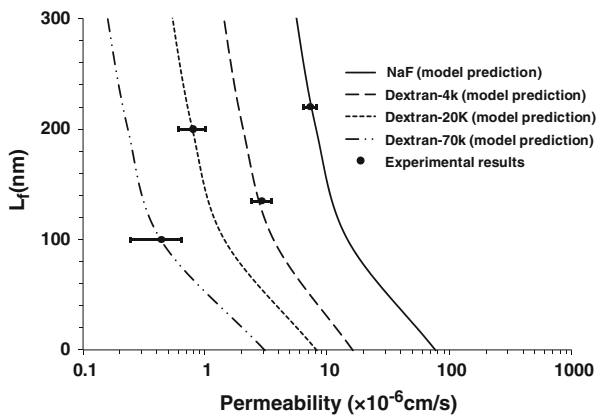
**FIGURE 4. Comparison of the permeability of bEnd3 monolayer ( $\blacklozenge$ ) to that of intact rat pial microvessel ( $\blacksquare$ ) to sodium fluorescein, dextran-4k, dextran-20k, and dextran-70k. Values were plotted as mean  $\pm$  SD. \*  $p < 0.001$ .**

#### Comparison of Permeability of bEnd3 Monolayer and that of Pial Microvessels to Neutral Solutes

Figure 4 compares the permeability of bEnd3 monolayer to various sized neutral solutes, NaF, dextran-4k, dextran-20k, and dextran-70k (diamonds), with that of intact rat pial microvessels to the same solutes (squares).<sup>47</sup> The ratios of permeability of bEnd3 ( $P_{\text{bEnd3}}$ ) to that of pial microvessels ( $P_{\text{pia}}$ ) are 3.0, 3.6, 3.8 and 3.4-fold, correspondingly, to NaF, dextran-4k, dextran-20k, and dextran-70k. This range of  $P_{\text{bEnd3}}$  to  $P_{\text{pia}}$  is much smaller than that of  $P_{\text{mesentery}}$  (measured in intact rat mesenteric microvessels) to  $P_{\text{pia}}$ , which is from 6 to 11-fold for the similar sized solutes.<sup>19,47</sup>

**TABLE 3. Anatomical parameters of bEnd3 monolayer in the model.**

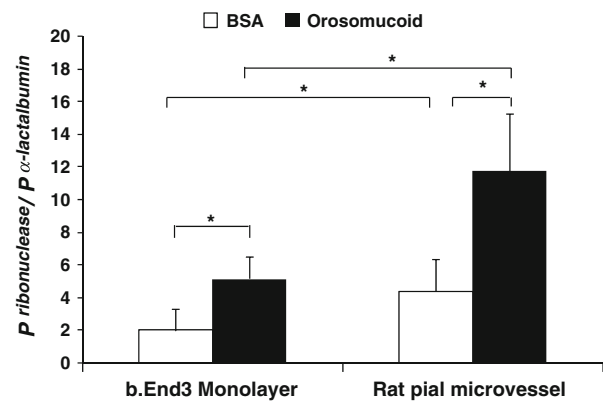
Fiber radius of surface glycocalyx layer <sup>34,38</sup> ( $r_f$ )	6 nm
Gap spacing between fibers of glycocalyx <sup>34,38</sup> ( $\Delta$ )	8 nm
Thickness of endothelial cells <sup>37</sup> ( $L$ )	700 nm
Distance between the junction strand and the front of the cleft <sup>17,37</sup> ( $L_1$ )	350 nm
Width of inter-endothelial cleft <sup>4</sup> ( $2B$ )	18 nm
Width of the small slit of the junction strand <sup>5,12</sup> ( $2B_s$ )	8 nm
Thickness of tight junction strand <sup>4</sup> ( $L_{jun}$ )	11 nm
Width of endothelial cells (measured in the present study) ( $2D$ )	20 $\mu$ m
Total cleft length per unit endothelial monolayer surface area (measured in the present study) ( $L_{jt}$ )	603 cm/cm <sup>2</sup>

**FIGURE 5. The permeability of bEnd3 monolayer to four different sized solutes as a function of the thickness of SGL,  $L_f$ , of the monolayer. The lines represent model predictions, and experimental results (circles) were plotted as mean  $\pm$  SD.**

Therefore, our results indicate that the bEnd3 monolayer carries the low solute permeability character of the BBB and thus can be a fairly good *in vitro* model for studying solute transport across the BBB.

#### Determination of Surface Glycocalyx Layer (SGL) Thickness $L_f$ of bEnd3 Monolayer

In order to predict the thickness of the SGL ( $L_f$ ) of bEnd3 monolayer, we have measured the solute permeability of the monolayer to four neutral solutes with characteristic sizes: sodium fluorescein (Stokes radius = 0.45 nm), dextran-4k (Stokes radius = 1.4 nm), dextran-20k (Stokes radius = 2.3 nm), and dextran-70k (radius = 3.5 nm). We also used a modified theoretical model from Fu *et al.*<sup>18</sup> to predict the  $L_f$  using the anatomical parameters of bEnd3 monolayer, either measured in the current study or from the literature. Table 3 summarizes the values for these parameters. The model geometry is shown in Fig. 1. The lines in Fig. 5 show the model predictions of the permeability to these four solutes as a function of  $L_f$ , while the filled circles

**FIGURE 6. Comparison of the ratios of  $P^{\text{ribonuclease}}/P^{\alpha\text{-lactalbumin}}$  of bEnd3 monolayer to that of pial microvessels<sup>46</sup> in 10 mg/mL BSA-Ringer solution (open columns) and in the solution added with 1 mg/mL orosomucoid (solid columns). The values were plotted as mean  $\pm$  SD. \*  $p < 0.05$ .**

represent the experimental results. From Fig. 5, we can see that for the best fit to the measured  $P$  to NaF, the thickness of the SGL,  $L_f$ , would be 215 nm, ranging from 195 to 260 nm when considering the deviation in the measured data; for Dextran-4k,  $L_f$  would be 140 nm, ranging from 110 to 160 nm; for Dextran-20k,  $L_f$  would be 200 nm, ranging from 150 to 260 nm; for Dextran-70k,  $L_f$  would be 100 nm, ranging from 85 to 180 nm. Overall, to account for the measured permeability data for all four solutes,  $L_f$  would be  $163 \pm 57$  nm, which is comparable to those found in the peripheral and cerebral microvessels.<sup>1,5</sup>

#### Comparison of Permeability of bEnd3 Monolayer and that of Pial Microvessels to Charged Solutes

Previously *in vivo* study has demonstrated that the charge carried by the SGL of the cerebral endothelium plays an important role in modulating the permeability of the BBB to charged solutes.<sup>46</sup> In the present study, we examined whether or not bEnd3 monolayer carries significant charge and has effect on the transport of charged solutes. If it does, how much is the charge density of the SGL of bEnd3 monolayer? Can the plasma glycoprotein, orosomucoid, modulate its permeability to charged solutes by adding the charge to the SGL, as it has been observed in the endothelium of the intact BBB?<sup>46</sup> To answer these questions, we measured the permeability of bEnd3 monolayer to the solutes with similar size but opposite charges: negatively charged  $\alpha$ -lactalbumin ( $-11$ ) and positively charged ribonuclease ( $+3$ ) in the presence and absence of orosomucoid. Figure 6 shows our results. The ratio of  $P^{\text{ribonuclease}}$  to  $P^{\alpha\text{-lactalbumin}}$  was about 2.0 in the absence of orosomucoid, which was less than that, 4.4, found in intact pial microvessels.<sup>46</sup> The difference is

partially due to the additional negative charge carried by the basement membrane sandwiched between the endothelium and the wrapping astrocytes of the intact BBB.<sup>14,22,27,30</sup> In the presence of orosomucoid, the ratio of  $P^{\text{ribonuclease}}$  to  $P^{\alpha\text{-lactalbumin}}$  was increased to 5.2, which is smaller than that measured in rat pial microvessels for the same reason as in the absence of orosomucoid.

#### Determination of Surface Glycocalyx Layer (SGL) Charge Density $C_{mf}$ of bEnd3 Monolayer

In order to estimate the charge density of the SGL,  $C_{mf}$ , of the bEnd3 monolayer, we combined the measured permeability of bEnd3 monolayer to negatively charged  $\alpha$ -lactalbumin (-11) and positively charged ribonuclease (+3) in a control solution of 10 mg/mL BSA-Ringer, with predictions from an electrodiffusion model modified from Fu *et al.*<sup>18</sup> using anatomical parameters of the bEnd3 monolayer (Table 3) and the SGL thickness  $L_f$  found from the previous section. The solid line in Fig. 7 shows our model prediction for the ratio of the permeability of the bEnd3 monolayer to ribonuclease to that to  $\alpha$ -lactalbumin as a function of the SGL charge density  $C_{mf}$ . The squares represent the measured permeability in the presence and absence of orosomucoid. To account for the measured ratio of  $P^{\text{ribonuclease}}$  to  $P^{\alpha\text{-lactalbumin}}$  of 2.0 in the absence of orosomucoid,  $C_{mf}$  would be 24 mEq/L, which is comparable to that of the SGL, ~30 mEq/L, at the endothelium of the intact pial microvessel.<sup>46</sup>

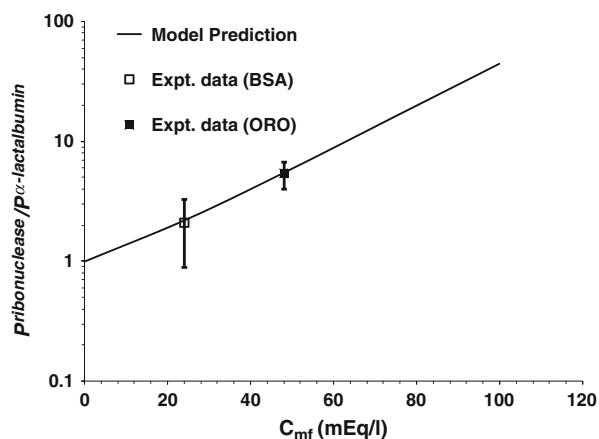


FIGURE 7. The ratio of  $P^{\text{ribonuclease}}$  to  $P^{\alpha\text{-lactalbumin}}$  as a function of charge density of SGL ( $C_{mf}$ ) of bEnd3 monolayer. The solid line represents the model prediction. The open square represents the measured ratio in 10 mg/mL BSA-Ringer (BSA), while the solid square represents the measured ratio in 1 mg/mL orosomucoid in BSA-Ringer (ORO). Experimental data were plotted as mean  $\pm$  SD.

#### Modulation of Permeability of bEnd3 Monolayer to Charged Solutes by Orosomucoid

Our recent study<sup>46</sup> demonstrated that the charge density of SGL of the intact pial microvessel increases from ~30 mEq/L in the absence of orosomucoid, to ~80 mEq/L in the presence of orosomucoid, by roughly 2.7-fold increase, in order to account for the increased ratio of  $P^{\text{ribonuclease}}$  to  $P^{\alpha\text{-lactalbumin}}$  under the orosomucoid treatment. For this *in vitro* BBB model of bEnd3 monolayer, our model (the line in Fig. 7) predicted that the charge density of the SGL  $C_{mf}$  would increase from ~25 mEq/L in the absence of orosomucoid to ~50 mEq/L in the presence of orosomucoid, by approximately 2-fold increase, in order to account for the measured ratios, the open square for the control and the solid square for the orosomucoid treatment. Although this increase ratio is slightly less than that in the intact pial microvessel, the added charge by orosomucoid to the SGL of bEnd3 is significant and it substantially modulates the transport of charged solutes.

#### Comparison of Permeability of bEnd3 Monolayer and that of Rat Pial Microvessels to QA $\beta$ CD Nanoparticles

We measured the permeability of both bEnd3 monolayer and rat pial microvessels to QA $\beta$ CD nanoparticles, designed as carriers for drug delivery to the central nervous system, to examine whether bEnd3 monolayer is a good *in vitro* model for transport study of drug carriers. The method for permeability measurement on rat pial microvessels has been published in our previous studies.<sup>39,40</sup> The permeability of bEnd3 monolayer and that of rat pial microvessels to QA $\beta$ CD nanoparticles are summarized in Fig. 8. Each QA $\beta$ CD sample is denoted as 1-W-N, where W and N represent the feeding molar ratios of choline and epichlorohydrin to  $\beta$ -CD, respectively.<sup>20</sup> Sample 1-15-0.5 has a

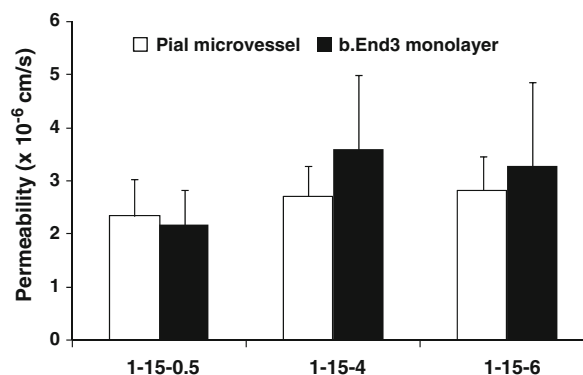


FIGURE 8. Comparison of the permeability of bEnd3 monolayer and that of rat pial microvessels to three samples of QA $\beta$ CD nanoparticles. The values were plotted as mean  $\pm$  SD.

zeta potential of  $-11.8$  ( $\zeta$ )<sup>c</sup>/mV, while sample 1-15-4 and sample 1-15-6 have zeta potential of 6 and 14 ( $\zeta$ )<sup>c</sup>/mV, respectively. Gil *et al.*<sup>20</sup> used the dynamic light scattering instrument to measure the QA $\beta$ CD nanoparticles at 50 mg/mL, pH 7.4 and 37 °C. The corresponding sizes were: 1-15-0.5:  $77.3 \pm 4.1$  (nm); 1-15-4:  $65.3 \pm 4.3$  (nm); 1-15-6:  $88.0 \pm 3.8$  (nm). They did not find particle aggregation at this concentration. When measuring the permeability, we diluted the nanoparticles to 100  $\mu$ g/mL and the aggregation was unlikely. The permeability of bEnd3 monolayer to sample 1-15-0.5, 1-15-4, and 1-15-6 was  $2.17 (\pm 0.66, \text{SD}, n = 6) \times 10^{-6}$  cm/s,  $3.60 (\pm 1.40, \text{SD}, n = 6) \times 10^{-6}$  cm/s, and  $3.27 (\pm 1.58, \text{SD}, n = 6) \times 10^{-6}$  cm/s, respectively, while that of rat pial microvessels was  $2.34 (\pm 0.70, \text{SD}, n = 9) \times 10^{-6}$  cm/s,  $2.71 (\pm 0.58, \text{SD}, n = 13) \times 10^{-6}$  cm/s, and  $2.83 (\pm 0.64, \text{SD}, n = 11) \times 10^{-6}$  cm/s, respectively. The permeability of bEnd3 monolayer to each QA $\beta$ CD nanoparticle shows no significant difference from that of rat pial microvessels ( $p > 0.05$ ). The permeability of bEnd3 monolayer to neutral Dextran-4k was  $2.91 \times 10^{-6}$  cm/s, which is slightly larger than that of the negatively charged 1-15-0.5, but smaller than that of positively charged 1-15-4, and 1-15-6. In contrast, the permeability of pial microvessels to neutral Dextran-4k was  $0.92 \times 10^{-6}$  cm/s,<sup>46</sup> which is roughly 1/3 of its permeability to these nanoparticles.

Because the endothelium of the BBB is wrapped by the basement membrane and astrocyte-foot processes, the resistance of the BBB would be larger for both paracellular and transcellular transport than that of the endothelium alone. That the permeability of the BBB to small molecule Dextran-4k is only 1/3 of that to the much larger nanoparticles suggests that instead of going through a paracellular pathway like Dextran-4k, these nanoparticles would go through a transcellular pathway across the BBB. In addition, there is no significant difference between the permeability of bEnd3 monolayer and that of pial microvessels to the QA $\beta$ CD nanoparticles. This implies that the trans-endothelial resistance is dominant in the nanoparticle transport across the BBB.

#### Future Studies

The TEER (transendothelial electric resistance) reflects the ion permeability of the endothelial layer. We measured the TEER of the bEnd3 monolayer (cultured for 4–5 days), which was  $23.6 \pm 2.7 \Omega\text{cm}^2$  (SD,  $n = 7$ ). This value is much smaller than  $\sim 1800 \Omega\text{cm}^2$ , the *in vivo* value for rat cerebral microvessels.<sup>10</sup> Koto *et al.*<sup>25</sup> measured the TEER of bEnd3 monolayer from 1 to 11 days after confluence (or 3–13 days of cell seeding). They found that the TEER increased with

days of culture, reaching the maximum of  $\sim 110 \Omega\text{cm}^2$  at day 8, and decreased afterwards. Compared to the *in vivo* TEER data, bEnd3 is not a good model for studying ion permeability. Contact co-culture with glial cells may be a good candidate since its TEER can reach  $\sim 1000 \Omega\text{cm}^2$ .<sup>28</sup> However, for the transport of larger molecules compared to ions, the resistance from the surface glycocalyx would be larger than that from the tight junction pores. Therefore, bEnd3 monolayer can serve as a fairly good *in vitro* model for investigating transport of relatively large molecules.

A recent study by Potter and Damiano<sup>34</sup> showed that the SGL was not present in *in vitro* assays of BAECs or HUVECs cultured in 100 to 150  $\mu$ m channels in collagen gels. There is also ample evidence from other studies that a substantial SGL exists *in vitro* depending on the culture conditions.<sup>6,40–42</sup> Under our culture conditions for bEnd3 cells, we tested the SGL as a functional transport barrier. To confirm its structural properties, we will perform immunostaining to relevant SGL components and confocal microscopy in the future.

In summary, the cultured cell monolayer of the immortalized mouse brain cell line, bEnd3, is able to maintain many characteristics of the BBB: low (paracellular) permeability to various sized solutes, suggesting fairly well-formed tight junctions; comparable thickness and the charge density of the SGL to that of the intact BBB endothelium; the charge of SGL can be modulated by orosomucoid in a similar way as in the intact BBB; demonstrating transcellular transport of large nanoparticles as observed in the intact BBB. Overall, the bEnd3 monolayer is a fairly good *in vitro* model for studying the solute and particle transport across the BBB.

#### ACKNOWLEDGMENTS

This work is supported in part by the National Science Foundation CAREER award, the Andrew Grove Foundation and PSC-CUNY research award of the City University of New York. We also thank Dr. Tao Lowe and Dr. Eun Seok Gil for the QA $\beta$ CD nanoparticles.

#### REFERENCES

- Adamson, R. H., and G. Clough. Plasma proteins modify the endothelial cell glycocalyx of frog mesenteric microvessels. *J. Physiol.* 445:473–486, 1992.
- Adamson, R. H., V. H. Huxley, and F. E. Curry. Single capillary permeability to proteins having similar size but



- different charge. *Am. J. Physiol.* 254(2 Pt 2):H304–H312, 1988.
- <sup>3</sup>Adamson, R. H., J. F. Lenz, and F. E. Curry. Quantitative laser scanning confocal microscopy on single capillaries: permeability measurement. *Microcirculation* 1(4):251–265, 1994.
  - <sup>4</sup>Adamson, R. H., J. E. Lenz, X. Zhang, G. N. Adamson, S. Weinbaum, and F. E. Curry. Oncotic pressures opposing filtration across non-fenestrated rat microvessels. *J. Physiol. Lond.* 557(3):889–907, 2004.
  - <sup>5</sup>Allt, G., and J. G. Lawrenson. Is the pial microvessel a good model for blood-brain barrier studies? *Brain Res. Brain Res. Rev.* 24(1):67–76, 1997.
  - <sup>6</sup>Barakat, A. I. Dragging along: the glycocalyx and vascular endothelial cell mechanotransduction. *Circ. Res.* 102(7):747–748, 2008.
  - <sup>7</sup>Brown, R. C., K. S. Mark, R. D. Egleton, J. D. Huber, A. R. Burroughs, and T. P. Davis. Protection against hypoxia-induced increase in blood-brain barrier permeability: role of tight junction proteins and NFkappaB. *J. Cell Sci.* 116(Pt 4):693–700, 2003.
  - <sup>8</sup>Brown, R. C., A. P. Morris, and R. G. O’Neil. Tight junction protein expression and barrier properties of immortalized mouse brain microvessel endothelial cells. *Brain Res.* 1130(1):17–30, 2007.
  - <sup>9</sup>Bruegger, D., M. Jacob, M. Rehm, *et al.* Atrial natriuretic peptide induces shedding of endothelial glycocalyx in coronary vascular bed of guinea pig hearts. *Am. J. Physiol. Heart Circ. Physiol.* 289(5):H1993–H1999, 2005.
  - <sup>10</sup>Butt, A. M. Effect of inflammatory agents on electrical resistance across the blood-brain barrier in pial microvessels of anaesthetized rats. *Brain Res.* 696(1–2):145–150, 1995.
  - <sup>11</sup>Cabrales, P., B. Y. Vazquez, A. G. Tsai, and M. Intaglietta. Microvascular and capillary perfusion following glycocalyx degradation. *J. Appl. Physiol.* 102(6):2251–2259, 2007.
  - <sup>12</sup>Cassella, J. P., J. G. Lawrenson, and J. A. Firth. Development of endothelial paracellular clefts and their tight junctions in the pial microvessels of the rat. *J. Neurocytol.* 26:547–575, 1997.
  - <sup>13</sup>Curry, F. E., J. C. Rutledge, and J. F. Lenz. Modulation of microvessel wall charge by plasma glycoprotein orosomucoid. *Am. J. Physiol.* 257(5 Pt 2):H1354–H1359, 1989.
  - <sup>14</sup>del Zoppo, G. J., and J. M. Hallenbeck. Advances in the vascular pathophysiology of ischemic stroke. *Thromb. Res.* 98(3):73–81, 2000.
  - <sup>15</sup>Farkas, E., and P. G. Luiten. Cerebral microvascular pathology in aging and Alzheimer’s disease. *Prog. Neurobiol.* 64(6):575–611, 2001.
  - <sup>16</sup>Fu, B. M., R. H. Adamson, and F. E. Curry. Test of a two-pathway model for small-solute exchange across the capillary wall. *Am. J. Physiol.* 274(6 Pt 2):H2062–H2073, 1998.
  - <sup>17</sup>Fu, B., and B. Chen. A model for the modulation of microvessel permeability by junction strands. *J. Biomech. Eng. Trans. ASME* 125(5):620–627, 2003.
  - <sup>18</sup>Fu, B. M., B. Chen, and W. Chen. An electrodiffusion model for effects of surface glycocalyx layer on microvessel permeability. *Am. J. Physiol. Heart Circ. Physiol.* 284(4):H1240–H1250, 2003.
  - <sup>19</sup>Fu, B. M., and S. Shen. Acute VEGF effect on solute permeability of mammalian microvessels in vivo. *Microvasc. Res.* 68(1):51–62, 2004.
  - <sup>20</sup>Gil, E. S., J. Li, H. Xiao, and T. L. Lowe. Quaternary ammonium beta-cyclodextrin nanoparticles for enhancing doxorubicin permeability across the in vitro blood-brain barrier. *Biomacromolecules* 10:505–516, 2009.
  - <sup>21</sup>Grabb, P. A., and M. R. Gilbert. Neoplastic and pharmacological influence on the permeability of an in vitro blood-brain barrier. *J. Neurosurg.* 82(6):1053–1058, 1995.
  - <sup>22</sup>Hamann, G. F., Y. Okada, R. Fritridge, and G. J. del Zoppo. Microvascular basal lamina antigens disappear during cerebral ischemia and reperfusion. *Stroke* 26(11):2120–2126, 1995.
  - <sup>23</sup>Haraldsson, B., and B. Rippe. Orosomucoid as one of the serum components contributing to normal capillary permselectivity in rat skeletal muscle. *Acta Physiol. Scand.* 129(1):127–135, 1987.
  - <sup>24</sup>Hawkins, B. T., and T. P. Davis. The blood-brain barrier/neurovascular unit in health and disease. *Pharmacol. Rev.* 57(2):173–185, 2005.
  - <sup>25</sup>Koto, T., K. Takubo, S. Ishida, *et al.* Hypoxia disrupts the barrier function of neural blood vessels through changes in the expression of claudin-5 in endothelial cells. *Am. J. Pathol.* 170(4):1389–1397, 2007.
  - <sup>26</sup>Kreuter, J. Influence of the surface properties on nanoparticle-mediated transport of drugs to the brain. *J. Nanosci. Nanotechnol.* 4(5):484–488, 2004.
  - <sup>27</sup>Leblond, C. P., and S. Inoue. Structure, composition, and assembly of basement membrane. *Am. J. Anat.* 185(4):367–390, 1989.
  - <sup>28</sup>Malina, K. C., I. Cooper, and V. I. Teichberg. Closing the gap between the in-vivo and in-vitro blood-brain barrier tightness. *Brain Res.* 1284:12–21, 2009.
  - <sup>29</sup>Matsumoto, K., K. Nishi, M. Kikuchi, *et al.* Alpha1-acid glycoprotein suppresses rat acute inflammatory paw edema through the inhibition of neutrophils activation and prostaglandin E2 generation. *Biol. Pharm. Bull.* 30(7):1226–1230, 2007.
  - <sup>30</sup>Miosge, N. The ultrastructural composition of basement membranes in vivo. *Histol. Histopathol.* 16(4):1239–1248, 2001.
  - <sup>31</sup>Moghimi, S. M., A. C. Hunter, and J. C. Murray. Long-circulating and target-specific nanoparticles: theory to practice. *Pharmacol. Rev.* 53(2):283–318, 2001.
  - <sup>32</sup>Nicolazzo, J. A., S. A. Charman, and W. N. Charman. Methods to assess drug permeability across the blood-brain barrier. *J. Pharm. Pharmacol.* 58(3):281–293, 2006.
  - <sup>33</sup>Omidi, Y., L. Campbell, J. Barar, D. Connell, S. Akhtar, and M. Gumbleton. Evaluation of the immortalised mouse brain capillary endothelial cell line, b.End3, as an in vitro blood-brain barrier model for drug uptake and transport studies. *Brain Res.* 990(1–2):95–112, 2003.
  - <sup>34</sup>Potter, D. R., and E. R. Damiano. The hydrodynamically relevant endothelial cell glycocalyx observed in vivo is absent in vitro. *Circ. Res.* 102(7):770–776, 2008.
  - <sup>35</sup>Sann, L., F. Bienvenu, J. Bienvenu, J. Bourgeois, and M. Bethenod. Evolution of serum prealbumin, C-reactive protein, and orosomucoid in neonates with bacterial infection. *J. Pediatr.* 105(6):977–981, 1984.
  - <sup>36</sup>Schnitzer, J. E., and E. Pinney. Quantitation of specific binding of orosomucoid to cultured microvascular endothelium: role in capillary permeability. *Am. J. Physiol.* 263(1 Pt 2):H48–H55, 1992.
  - <sup>37</sup>Schulze, C., and J. A. Firth. Interendothelial junctions during blood-brain-barrier development in the rat—morphological-changes at the level of individual tight junctional contacts. *Dev. Brain Res.* 69(1):85–95, 1992.
  - <sup>38</sup>Sorensson, J., G. L. Matejka, M. Ohlson, and B. Haraldsson. Human endothelial cells produce orosomucoid, an important component of the capillary barrier. *Am. J. Physiol.* 276(2 Pt 2):H530–H534, 1999.

- <sup>39</sup>Squire, J. M., M. Chew, G. Nneji, C. Neal, J. Barry, and C. Michel. Quasi-periodic substructure in the microvessel endothelial glycocalyx: a possible explanation for molecular filtering? *J. Struct. Biol.* 136(3):239–255, 2001.
- <sup>40</sup>Stevens, A. P., V. Hlady, and R. O. Dull. Fluorescence correlation spectroscopy can probe albumin dynamics inside lung endothelial glycocalyx. *Am. J. Physiol. Lung Cell. Mol. Physiol.* 293(2):L328–L335, 2007.
- <sup>41</sup>Tarbell, J. M., and M. Y. Pahakis. Mechanotransduction and the glycocalyx. *J. Intern. Med.* 259(4):339–350, 2006.
- <sup>42</sup>Thi, M. M., J. M. Tarbell, S. Weinbaum, and D. C. Spray. The role of the glycocalyx in reorganization of the actin cytoskeleton under fluid shear stress: a “bumper-car” model. *Proc. Natl. Acad. Sci. USA* 101(47):16483–16488, 2004.
- <sup>43</sup>Ueno, M., H. Sakamoto, Y. J. Liao, *et al.* Blood-brain barrier disruption in the hypothalamus of young adult spontaneously hypertensive rats. *Histochem. Cell Biol.* 122(2):131–137, 2004.
- <sup>44</sup>Ueno, M., H. Sakamoto, H. Tomimoto, *et al.* Blood-brain barrier is impaired in the hippocampus of young adult spontaneously hypertensive rats. *Acta Neuropathol.* 107(6):532–538, 2004.
- <sup>45</sup>Weinbaum, S., X. Zhang, Y. Han, H. Vink, and S. C. Cowin. Mechanotransduction and flow across the endothelial glycocalyx. *Proc. Natl. Acad. Sci. USA* 100(13):7988–7995, 2003.
- <sup>46</sup>Yuan, W., G. Li, and B. Fu. Modulation of the blood-brain barrier permeability by plasma glycoprotein orosomucoid. *FASEB J.* 23:1020.1, 2009.
- <sup>47</sup>Yuan, W., Y. Lv, M. Zeng, and B. M. Fu. Non-invasive measurement of solute permeability in cerebral microvessels of the rat. *Microvasc. Res.* 77(2):166–173, 2009.